Scanning Microscopy

Volume 2 | Number 1 Article 33

9-16-1987

Scanning Electron Microscopy and Electron Probe Microanalyses of the Crystalline Components of Human and Animal Dental Calculi

R. Z. LeGeros
New York University Dental Center

I. Orly
New York University Dental Center

J. P. LeGeros
New York University Dental Center

C. Gomez
New York University Dental Center

J. Kazimiroff
New York University Dental Center

Scanning Electron Microscopy and Electron Probe Microanalyses of the Crystalline Components of Human and Animal Dental Calculi

Authors

R. Z. LeGeros, I. Orly, J. P. LeGeros, C. Gomez, J. Kazimiroff, T. Tarpley, and B. Kerebel

Scanning Microscopy, Vol. 2, No. 1, 1988 (Pages 345-356)
Scanning Microscopy International, Chicago (AMF O'Hare), IL 60666 USA

0891-7035/88$3.00+.00

SCANNING ELECTRON MICROSCOPY AND ELECTRON PROBE MICROANALYSES OF THE CRYSTALLINE COMPONENTS OF HUMAN AND ANIMAL DENTAL CALCULI

R.Z. LeGeros[1]*, I. Orly[1], J.P. LeGeros[1], C. Gomez[1]
J. Kazimiroff[1], T. Tarpley[2], and B. Kerebel[3]

[1]New York University Dental Center, New York, NY 10010
[2]Georgetown University, Dept. of Pathology, Washington, DC 20007
[3]U-225, INSERM, UERd'Odontologie, 44042 Nantes, France

(Received for publication April 06, 1987, and in revised form September 16, 1987)

Abstract

A review of the use of scanning electron microscopy (SEM) and electron probe microanalyses in the study of dental calculus showed that such studies provided confirmatory and supplementary data on the morphological features of human dental calculi but gave only limited information on the identity of the crystalline or inorganic components.

This study aimed to explore the potential of combined SEM and microanalyses in the identification of the crystalline components of the human and animal dental calculi. Human and animal calculi were analyzed. Identification of the crystalline components were made based on the combined information of the morphology (SEM) and Ca/P molar ratios of the crystals with the morphology and Ca/P molar ratio of synthetic calcium phosphates (brushite or DCPD; octacalcium phosphate, OCP; Mg-substituted whitlockite, β-TCMP; CO_3-substituted apatite, (CHA); and calcite.

SEM showed similarities in morphological features of human and animal dental calculi but differences in the forms of crystals present. Microanalyses and crystal morphology data suggested the presence of $CaCO_3$ (calcite) and CHA in the animal (cat, dog, tiger) and of OCP, β-TCMP and CHA in human dental calculi. X-ray diffraction and infrared (IR) absorption analyses confirmed these results.

This exploratory study demonstrated that by taking into consideration what is known about the crystalline components of human and animal dental calculi, combined SEM and microanalyses can provide qualitative identification.

Key Words: Dental calculi, apatite, octacalcium phosphate, Mg-substituted tricalcium phosphate (β-TCMP), scanning electron microscopy, infrared absorption spectroscopy, microanalysis, X-ray diffraction.

*Address for correspondence:
R.Z. LeGeros
New York University Dental Center,
345 East 24th St.
New York, NY 10010
Phone No.: (212) 998-9570

Introduction

Human dental calculus forms above and/or below the gums (supra- and/or sub-gingivally) resulting from the mineralization of the bacterial plaque adsorbed on the tooth (enamel and/or cementum) surfaces [11,38,41,46]. Supra-gingival calculi are usually found where the ducts of the large salivary glands exit into the oral cavity; while sub-gingival calculi are not localized at the exits of the salivary ducts and may or may not be continuous with supra-gingival calculi [5,11,38]. Dental calculus, like other calcified tissues, consists of organic and inorganic crystalline components.

Combined data from reported results of chemical [9,12,36], x-ray diffraction [9,12,13,20,23,26,36,42,43,49,51], transmission electron microscopy (TEM) [8,44,46], electron diffraction [44], and microdiffraction [16] analyses allowed the precise identification of the crystalline components of human and some animal (dog, sheep, miniature pig) dental calculi. The combined data indicated that human dental calculi consists of four types of calcium phosphates: (a) brushite or dicalcium phosphate dihydrate, DCPD, $CaHPO_4.2H_2O$; (b) octacalcium phosphate, OCP, $Ca_8H_2(PO_4)_6.5H_2O$; (c) whitlockite or Mg-substituted tricalcium phosphate, β-TCMP, $(Ca,Mg)_3(PO_4)_2$; and (d) carbonate (CO_3-) substituted apatite, CHA (Table 1). The relative abundance of the different types of calcium phosphates was reported to depend on several factors: age of calculus, location in the tooth (supra- or sub-gingival), location of the tooth (anterior or posterior), location within the sample (in contact with saliva or in contact with the tooth, enamel or cementum surfaces) (Table 1). For example: DCPD occurs least frequently, usually associated with "young" (e.g., 3-day old) supra-gingival calculus [7,9,12,13,46]; OCP was often associated with supra- but not with sub-gingival calculus [5,9,46]; β-TCMP, although found in both supra- and sub-gingival calculi, was consistently predominant in sub-gingival calculi [7,9,12]; CHA was found in all types and ages of calculi [9,11-13,20,24,26,36,44,46,49]. Animal dental calculi were principally supra-gingival [51]. The crystalline components of dog [26], sheep [26] and miniature pig [51] dental calculi consisted principally of calcium carbonate, $CaCO_3$ (calcite form) mixed with small amounts of CHA.

The use of scanning electron microscopy (SEM) in the investigations of the crystalline components of human dental calculi was first reported by Kerebel [17,18] who observed large cuboidal crystals in some

calculus samples. Lustman et al. [37] demonstrated the presence of various crystal forms: needle-like or elongated shapes, platelet forms, cuboidal forms, and assumed these different morphologies (except for cuboidal, which they considered as possible artifacts) represent the different types of calcium phosphates previously identified by other investigators using x-ray diffraction and (TEM) [8,9,12,13,20,23,26,42,44,46]. Neither Kerebel, nor Lustman et al., identified the crystalline components of the calculi examined by SEM. For characterization of morphological features of human dental calculi, SEM [1,14,17,18,27,37] confirmed earlier observations obtained from histological and TEM studies [5,38,39,52]. Such morphological features included: (a) presence of two types of mineralization centers, associated and non-associated with bacteria, as reported by Schroeder using TEM [46]; (b) differences in microbial population between supra-and sub-gingival human calculi - i.e., heterogeneous flora (mixture of cocci, rods and filaments) in sub-gingival calculus and mainly filamentous microorganisms in supra-gingival calculi [1,7,14,17,18,37]; (c) presence of channels in sodium hypochlorite-treated calculus indicated that calcification was primarily intermicrobial rather than within the microorganisms [7]; (d) modes of calculus attachment to human tooth being characterized by the presence of cuticular attachment, mechanical locking into undercuts, and direct attachment of the calculus matrix to the tooth surface frequently making the calculus-cementum interface indistinguishable from either the calculus or the cementum areas [2] confirming earlier histological findings [39,52]. (The excellent review by Jones [15] gives an extensive treatment of the past and current morphological features of human dental calculi from SEM studies).

Recent SEM studies on the comparative surface characteristics of sound, remineralized enamel and dental calculi were reported by Hoyer et al. [10]. Hoyer's study also used electron probe microanalysis on ten integrated areas of 400 μm^2 and reported a Ca/P molar ratio (calculated by the authors from the

Table 1: Calcium Phosphates in Human and Animal Dental Calculi

Calcium Phosphates	Occurrence
Brushite, dicalcium phosphate dihydrate, DCPD, $CaHPO_4.2H_2O$	'young' supra-gingival calculi
Octacalcium phosphate, OCP, $Ca_8H_2(PO_4)_6(OH)_2$	frequently in supra- occasionally in sub-gingival.
Whitlockite, Mg-substituted tricalcium phosphate, β-TCMP, $(Ca,Mg)_3(PO_4)_2$	both in supra- and consistently in sub-gingival
CO_3-substituted apatite, CHA, *$(Ca,Mg,Na,K)_{10}(PO_4,CO_3)_6(OH,Cl,F)_2$	both in supra- and sub-gingival and in all ages; minor component mixed with $CaCO_3$ in animal dental calculi.

*Approximate chemical composition.

Table 2: Ca/P Molar Ratios of Synthetic Calcium Phosphates.

Calcium Phosphates	Ca/P
DCPD, $CaHPO_4.2H_2O$	1.0
OCP, $Ca_8H_2(PO_4)_6.5H_2O$	1.33
β-TCMP, $(Ca,Mg)_3(PO_4)_2$	1.26-1.47*
CHA, $(Ca,Na)_{10}(PO_4,CO_3)_6(OH)_2$	1.65 to 2.33**

*Depending on the amount of Mg-for-Ca substitution.
**Depending on the amount of CO_3-for-PO_4 and Na-for-Ca substitution.

Table 3: Identification of Major Crystalline Components in Human (HDC) and Animal (ADC) Dental Calculi using Electron Probe Microanalysis

Sample	Region	Ca/P(molar)*	Identification**
HDC1	1C	1.54	β-TCMP
	2C	1.55	β-TCMP
	3C	1.43	β-TCMP
	4C	1.56	β-TCMP
	5C	1.41	β-TCMP
	6C	1.66	CHA
	7C	1.52	β-TCMP
	8C	1.41	β-TCMP
	9C	1.96	CHA
	10C	1.65	CHA
HDC1	1S	1.61	CHA
	2S	1.39	OCP
	3S	1.43	β-TCMP
	4S	1.50	β-TCMP
	5S	1.57	β-TCMP
	6S	1.39	OCP
	7S	1.62	CHA
	8S	1.53	β-TCMP
	9S	1.52	β-TCMP
	10S	1.54	β-TCMP
ADC1	1C	6.40	$CaCO_3$
	2C	1.73	CHA
	3C	1.77	CHA
	4C	1.81	CHA
	5C	6.22	$CaCO_3$
	6C	1.72	CHA
	7C	4.05	$CaCO_3$
	8C	5.75	$CaCO_3$
	9C	7.30	$CaCO_3$
	10C	1.79	CHA
ADC1	1S	28.69	$CaCO_3$
	2S	2.73	CHA
	3S	2.39	CHA
	4S	14.88	$CaCO_3$
	5S	23.02	$CaCO_3$
	6S	6.97	$CaCO_3$
	7S	31.68	$CaCO_3$
	8S	29.88	$CaCO_3$
	9S	13.91	$CaCO_3$
	10S	26.88	$CaCO_3$

C=in contact with cementum; S=in contact with saliva
*Calculated from microanalysis data
**Based on presence of Mg from microanalysis data and approximate Ca/P molar ratio of synthetic calcium phosphates (Table 2).

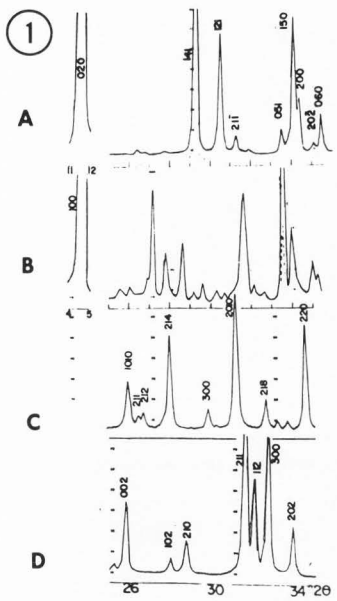

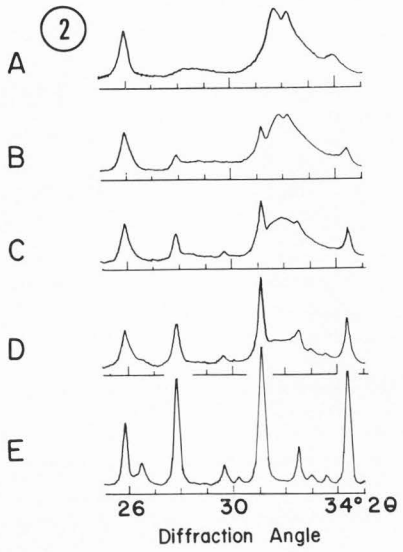

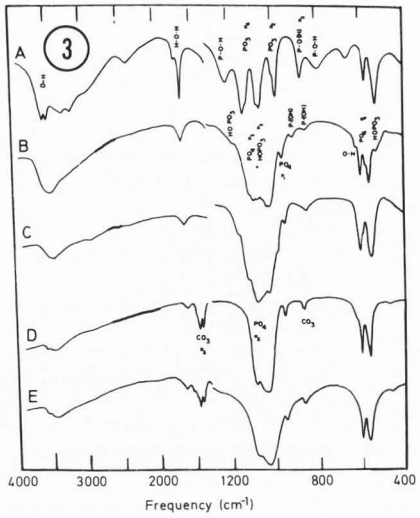

Fig.1. X-ray diffraction patterns of synthetic calcium phosphates: (A) DCPD, $CaHPO_4.2H_2O$; (B) OCP, $Ca_8H_2(PO_4)_6.5H_2O$; (C) Mg-substituted whitlockite or β-TCMP, $(Ca,Mg)_3(PO_4)_2$; (D) apatite. All synthetic materials were prepared in gel systems [23,25] but may also be prepared by precipitation [19,20-22;27-29,31-35].

Fig.2. Effect of solution Mg/Ca on the formation of Mg-substituted whitlockite or β-TCMP. Prepared by precipitation at 60°C, (A) without Mg; (B) solution Mg/Ca = 5/95; (C) 10/90; (D) 15/85; (E) 20/80.

Fig.3. Infrared (IR) absorption spectra of synthetic calcium phosphates (A) to (D) and biological calcium phosphate, CO_3-containing apatite, CHA. (A) DCPD; (B) OCP; (C) β-TCMP; (D) CHA; (E) human enamel apatite.

reported weight ratios) ranging from 0.91 to 1.62 in dental calculi, compared to 1.50 to 1.83 in sound, and 1.38 to 1.62 in remineralized enamel. No attempts were made to identify possible types of calcium phosphates present in the human dental calculi.

The review of the previous applications of SEM in the studies of human dental calculi (only human specimens have been heretofore investigated) revealed that SEM studies [1,2,7,10,14,17,37], even combined with microanalysis [10], did not contribute significantly to the identification of the crystalline inorganic components, compared to the information provided by x-ray diffraction, TEM, and infrared (IR). Therefore, the purpose of our current studies was to explore the possibility of utilizing combined SEM and microanalyses in the identification of the crystalline components of human and animal dental calculi.

Materials and Methods

Human dental calculus samples were obtained from adults (30 to 50 years old). Animal dental calculus samples were obtained from adult dogs, cats and a tiger. The samples were rinsed well with distilled water and air dried. For x-ray diffraction and IR analyses, the samples were powdered to pass 300 mesh. X-ray diffraction analyses were performed on a Philips APD 3520, using Ni-filtered Cu radiation generated at 40 kV and 20 mA, using silicon as standard. IR absorption analyses were performed on sample/KBr pellets (2mg sample / 300mg KBr, pressed with 700 kg/cm^2) using a Perkin-Elmer 983G. Assignment of absorption bands in the IR spectra are based on earlier studies (6,20,25,29,31,32).

SEM examinations and energy dispersive X-ray analyses (EDX) were performed on a Hitachi S-450 instrument. For SEM studies, the specimens were cemented on Al holders with colloidal silver and coated with both carbon and gold, and examined at 15 kV. For EDX, the specimens were cemented with carbon glue and coated with carbon. Calibration was performed before each analysis using Al and Cu K peaks. The system was programmed to identify Mg, Ca, and P peaks, to subtract a background spectrum from the spectrum of interest, and to print out the values of the appropriate peaks. The parameters used were 10 kV, 5° tilt angle, and 34° take off angle. Data were collected over 60 seconds. For each crystal specimen, areas of similar crystal form were chosen, and data accumulated on ten points (of 1 μm diameter each) on the saliva contact surface and ten points on the tooth contact surface. Ca/P, Mg/Ca molar ratios were calculated for each point and relationships (e.g., Mg = f(Ca/P) were tested using a computer program.

Synthetic $CaCO_3$ (calcite), DCPD, OCP, β-TCMP and CHA prepared as previously described [19-23,25-31,34,35] were characterized using x-ray diffraction (Figs. 1 and 2), IR (Fig. 3), crystal morphologies (Fig. 4), and Ca/P molar ratios determined from analyses of calcium (using atomic absorption spectrophotometry) and phosphate (using calorimetric methods). The crystal morphologies (Fig. 4) and Ca/P molar ratios (Table 2) of the synthetic materials were compared with those of the morphologies (Figs. 5,6) and Ca/P molar ratios (Table 3) of the crystalline components of the human and dental calculi. X-ray diffraction patterns (Figs. 7,8) and IR spectra (Fig. 9) of the calculi were compared to those of synthetic materials (Figs. 1,2,3) to confirm SEM / EDX identification.

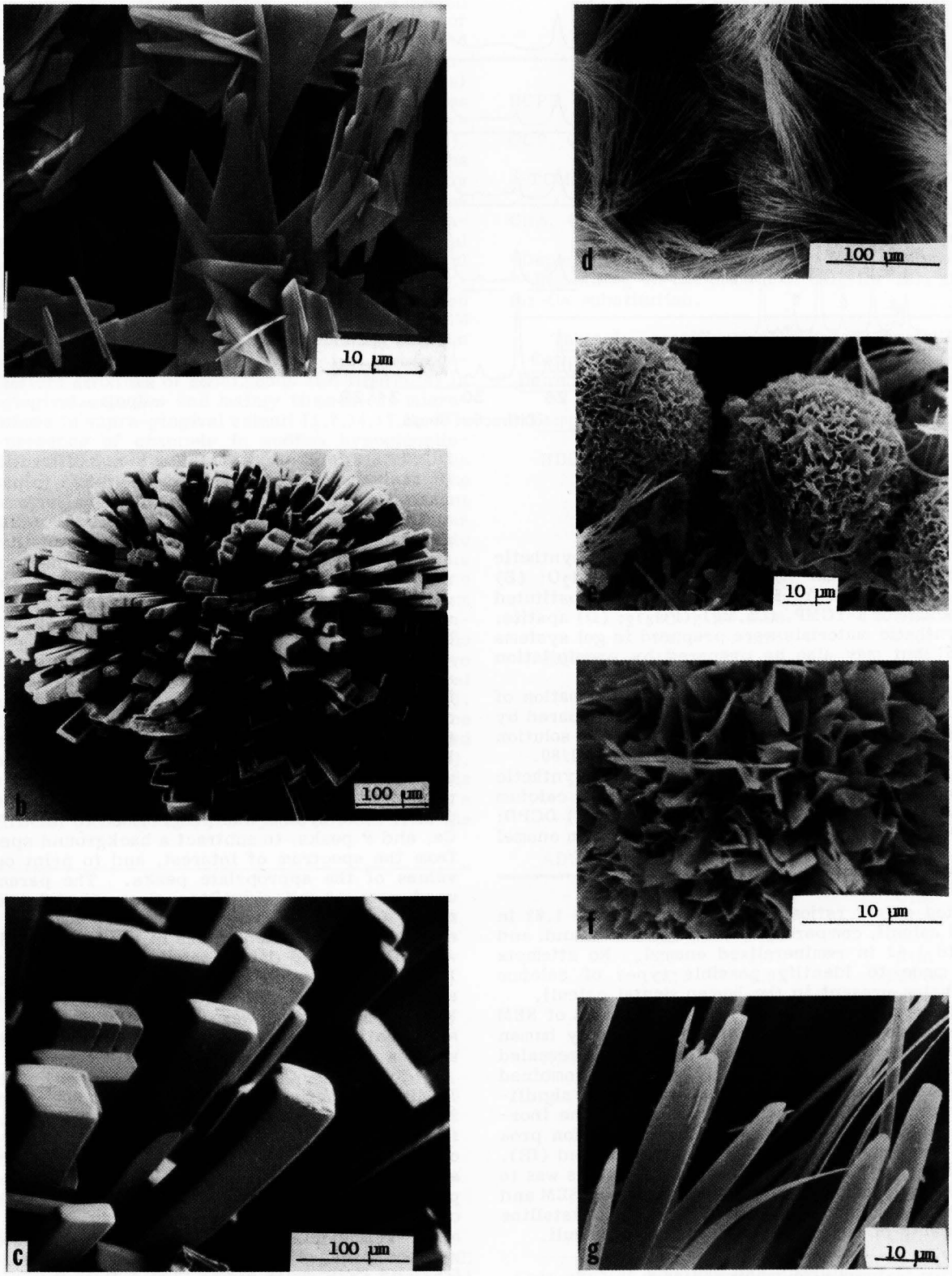

Fig.4. SEM of synthetic calcium phosphates. (a) DCPD showing typical triangular plate habits when obtained from systems containing only calcium and phosphate ions; (b) and (c), DCPD grown in the presence of pyrophosphate causing modification of morphology; (d) OCP growing as long needles growing from a common center as spheres or fan-like aggregates; (e) and (f) OCP growing as aggregates of plates in a sphere; (g) individual crystals from (d).

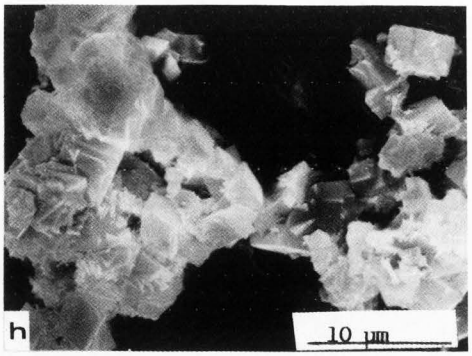

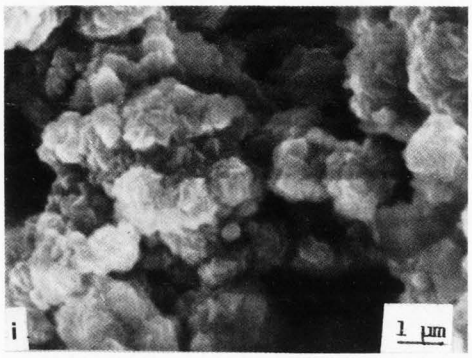

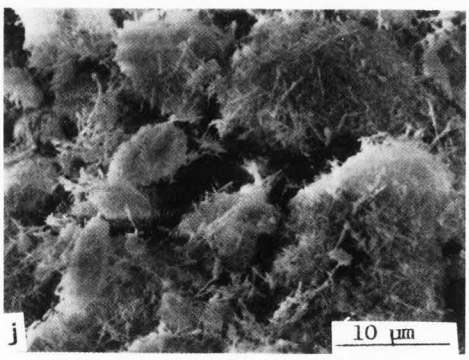

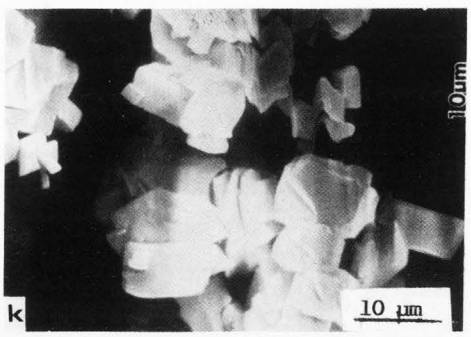

Fig.4 (continued). SEM of synthetic calcium phosphates (h,i,j) and calcium carbonate (k). (h) and (i), Mg-substituted whitlockite, β-TCMP; (j) CO_3-substituted apatite, CHA, containing 1 wt% CO_3; (k) calcium carbonate, $CaCO_3$, calcite form.

Results

SEM Investigations

Synthetic calcium phosphates and calcium carbonate. DCPD obtained by precipitation or from gel systems [23,25,31] usually assumes a plate-like or tabular form (Fig. 4a); when grown in the presence of pyrophosphate, the typical morphology is modified [23,25,31] as shown in Figs. 4b,4c. OCP obtained by precipitation [19,22,29] or in gel systems [25, 31] consists of long needles (Figs. 4d,4g) or plates (Figs. 4c,4f) originating from a common center (Figs. 4d,4e) as spheres (Fig. 4e) or fan-like agglomerates (Fig. 4d). β-TCMP obtained by precipitation [19,21,17] or by hydrolysis of DCPD [3] or $CaHPO_4$ [21,27] in solutions with Mg/Ca molar ratios exceeding 0.2 are cuboidal (Figs. 4h,4i). Apatite prepared by precipitation or hydrolysis assumes the morphology of long thin needles (Fig. 4j); CO_3-containing apatites, CHA, can assume morphologies from needle-like (Fig. 4j) to rods to equi-axed crystals depending on the amount of CO_3 incorporated [19,33]. CHA crystals (even with very low CO_3 content, about 0.5 wt%) are much smaller than the needle-like crystals of OCP (cf Figs. 4d,4g and 4j). Synthetic $CaCO_3$ (calcite) prepared by precipitation [26] are cuboidal in form (Fig. 4k).

Human dental calculi. Morphological features observed included: presence of microorganisms of cocci and rods as shown by calcified forms (Fig. 5b), and channels or holes vacated by microorganisms (Fig. 5d); calcophoritic calcifications (Fig. 5c), aggregated plates (Figs. 5e,5f,5h) and cuboidal forms of varying sizes (Figs. 5g,5i). Comparing the crystal morphologies of synthetic calcium phosphates (Fig. 4) with those observed in dental calculi (Figs. 5e to 5i), the crystalline components were tentatively identified as follows: clusters of platelets (Figs. 5f,5h), OCP; fan-like aggregation, OCP; cuboidal crystals (Figs. 5g, 5i), β-TCMP. Since CHA crystals are much smaller even when prepared at 95°C (Fig. 4i), the crystals in calcophoritic and dense calcifications (Figs. 5c,5f) may be assumed to consist of CHA, since the apatites usually associated with human dental calculi have crystallinity (reflecting crystal size) similar to that of bone or dentin [19,20] which would be similar to that of synthetic apatite prepared at 37 or 60°C (Figs. 2a, 2b).

Animal dental calculi. Some of the morphological features of the animal, e.g., cat (Fig. 6b), dog (Fig. 6c), and tiger (Fig. 6d) dental calculi resembled those of human dental calculi (Fig. 5). For example, presence of microorganisms (Figs. 6b,6c), channels or pores (Figs. 6d), and crystals (Figs. 6e to 6h). The crystals varied in size, the form resembling those of synthetic calcite (Fig. 4k compared with Figs. 6e to 6h).

Electron probe microanalyses (EDX)

When the results of semi-quantitative microanalyses (Mg, Ca, P) were classified according to the distribution of Ca/P molar ratios, a considerable difference was observed between human and animal calculi (Figs. 7a,b and Table 3): a greater number of regions in human dental calculi with Ca/P between 1.3 to 1.7 were found, while a greater number of regions of Ca/P above 2.5 were found in animal dental calculi. This observation suggested differences in the composition of the crystalline components in human and animal calculi. Examination of the relationship between the Mg concentration (wt%) and Ca/P

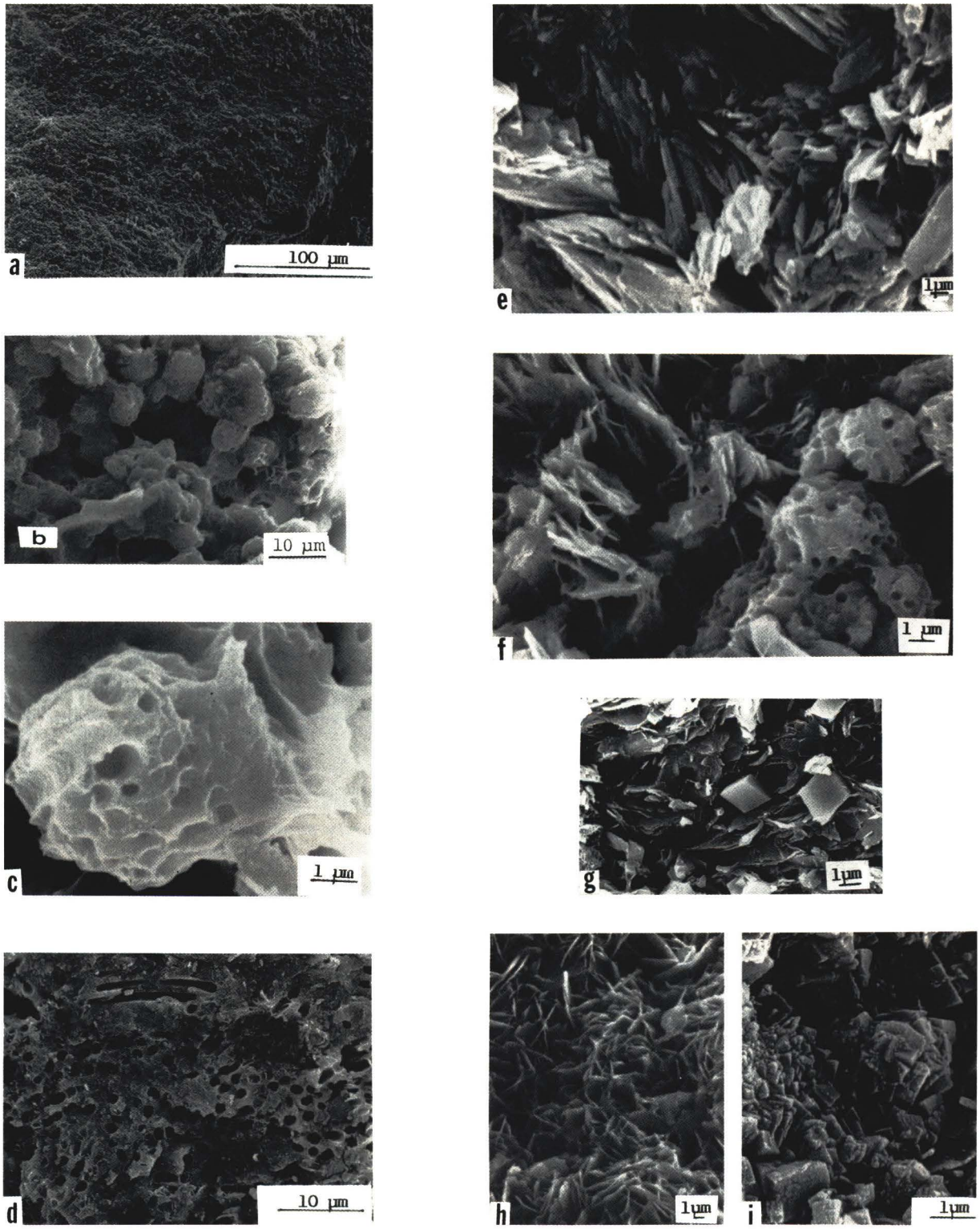

Fig.5. SEM of human dental calculi: (a) surface; (b) calcified spherical masses showing pores; (c) magnified region of (b); (d) densely calcified areas showing holes of different shapes; (e) crystals in fan-like aggregations from fractured section; (f)two mineralization centers: associated with bacteria (porous region), and non-associated with bacteria (dense region); (g) large cuboidal crystals on densely mineralized areas; (h) aggregation of plates; (i) cuboidal crystals of varying size and states of aggregation.

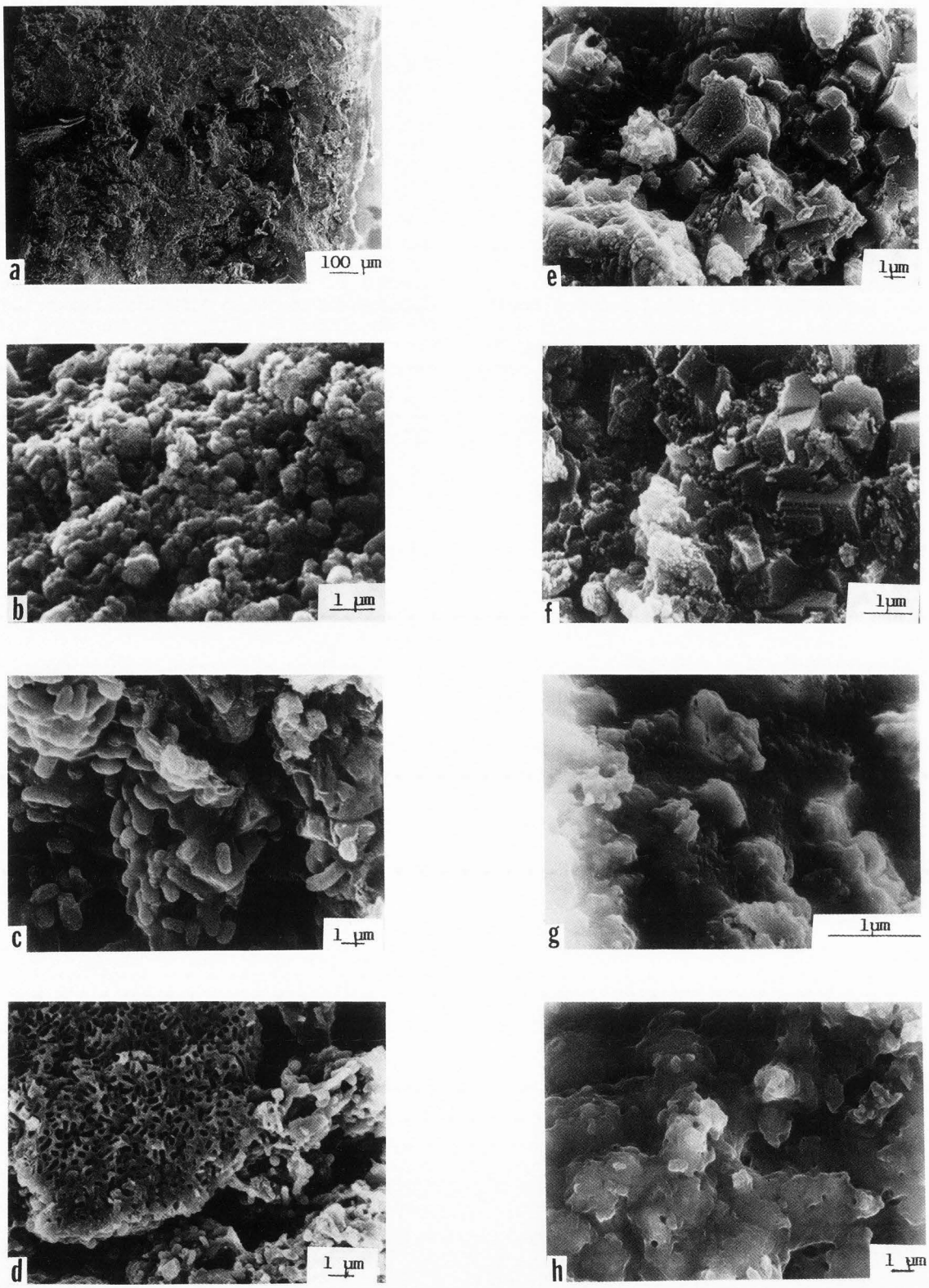

Fig.6. SEM of animal dental calculi showing surface (a); calcified microorganisms in cat (b) and in dog (c), and the presence of pores (d); and cuboidal crystals in dog (e) and (f), and in cat (g) and (h). As in human dental calculi (Fig. 5), the animal dental calculi show two types of mineralization centers, associated with microorganisms (b) and (c), and not associated with calcified microorganisms (d) to (h).

molar ratio showed a correlation between Mg and Ca/P of 1.4 to 1.6 in human (Figs. 8b, 8c), while in animal calculi (Fig. 8a) no significant correlation can be established. From the known Ca/P molar ratios of synthetic calcium phosphates (Table 2) and the absence of phosphate in $CaCO_3$, the composition of each point (diameter = 1 μm) in the human dental calculi was approximated as follows: Ca/P close to 1.3, OCP; close to 1.4, β-TCMP; close to 1.7, CHA (Table 3). Since no points gave a Ca/P approximating 1, DCPD was assumed to be absent. (SEM did not show any DCPD-like forms, as in Figs. 4a to 4c, either). In animal dental calculi, the composition of each point was approximated as follows: Ca/P less than 2.5, CHA; above 3 up to 15, CHA and $CaCO_3$, the CHA/$CaCO_3$ distribution decreasing with increasing Ca/P; Ca/P above 15, principally a non-phosphatic calcium compound, presumably $CaCO_3$ (Table 3). The identification of $CaCO_3$ and other non-phosphatic calcium compound was based on the reported presence of $CaCO_3$ (calcite form) in animal calculi: dog, sheep, and miniature pig [26,51].

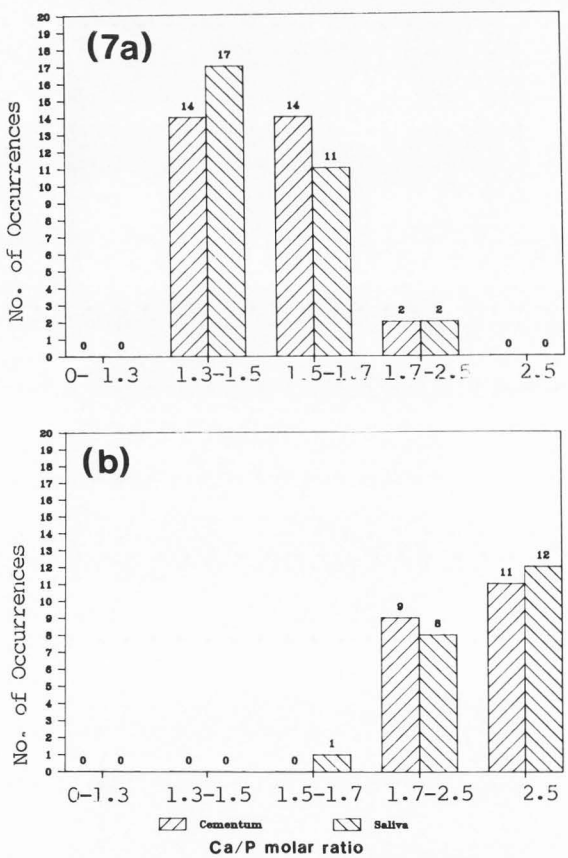

Fig.7. (above) Distribution of Ca/P molar ratios in human (a), and animal (b), dental calculus.

Fig.8. (right) Correlation between Mg content (wt %) and Ca/P molar ratio (from microanalysis data) for animal (a), and human (b, and a region of b magnified in c) dental calculus. No significant correlation was observed in animal dental calculi (a). A significant correlation was observed in human calculi, especially in the region of Ca/P molar ratio of 1.4 to 1.6 (c), which approximates the ratio for β-TCMP.

X-ray diffraction analyses

X-ray diffraction patterns of samples of human dental calculi (Figs. 9 and 10) showed the presence of OCP, β-TCMP, apatite (whether or not the apatite component was CHA cannot be determined from the x-ray diffraction pattern of poorly crystalline apatitic material alone), but not of DCPD; while those of animal dental calculi showed the presence of calcite and apatitic material in dog and cat (Figs. 10A, 10B). The apatite component of animal calculi was less crystalline (or much smaller in size) than the apatite in human (Figs. 9 and 10C, compared with 10A,10B). The apatite in human calculi is less crystalline than synthetic apatite prepared at 95°C (Fig. 1D) but a little more crystalline than those prepared at 37°C (Fig. 2A). ("Crystallinity" is reflected in the sharpness of the x-ray diffraction peaks; the broader the peaks, the lower the crystallinity or the smaller the crystallite size; the sharper the peaks, the greater the crystallinity, the larger the crystallite size).

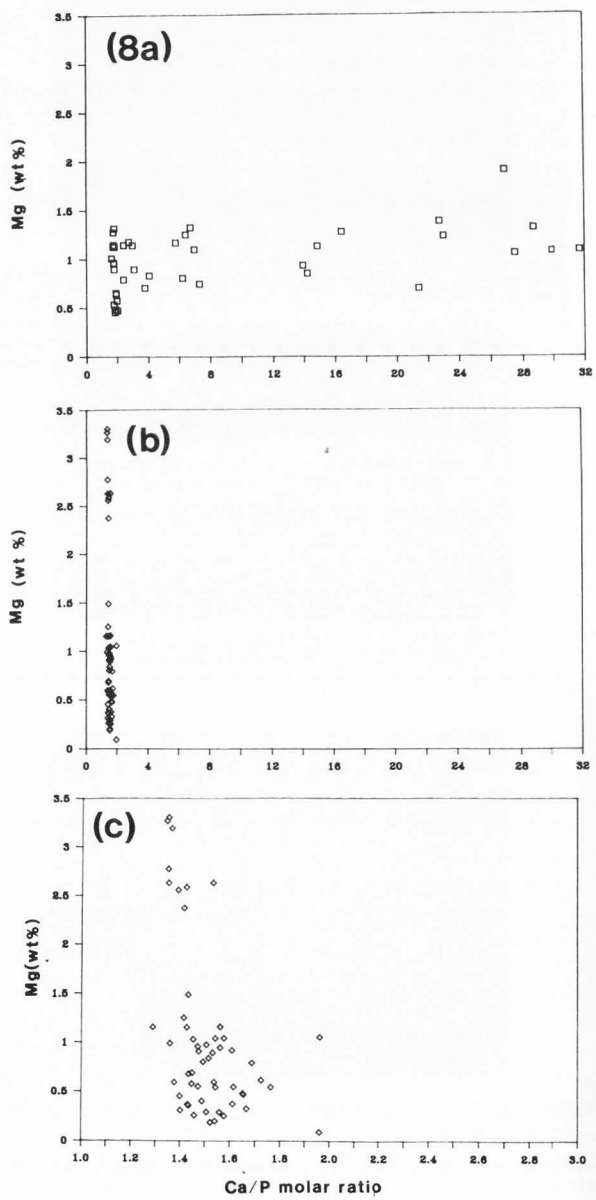

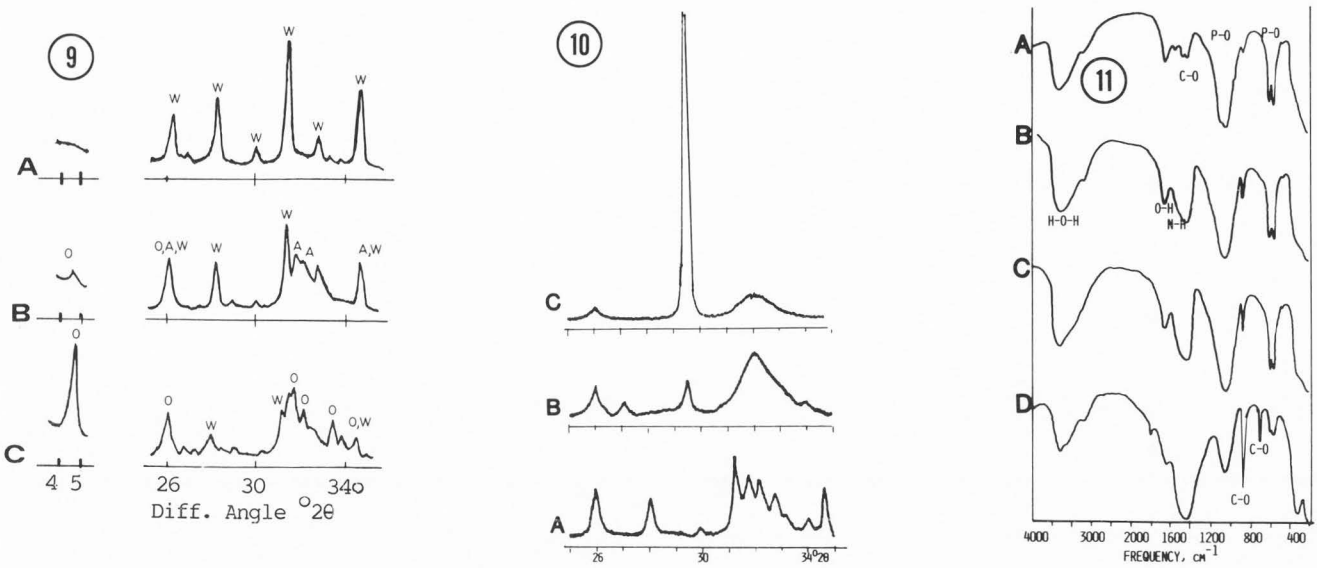

Fig.9. X-ray diffraction patterns of human dental calculi showing the presence principally of β-TCMP, W (A), mixture of OCP, O, apatite, A, and β-TCMP, W (B); principally OCP, O, mixed with β-TCMP, W (C).
Fig.10. X-ray diffraction patterns of calculi of human (A), cat (B) and dog (C). The human calculi (A) contains a mixture of calcium phosphates, β-TCMP, OCP and apatite; the cat calculi, a mixture of calcite and apatite (B); and the dog calculi, predominantly calcite and small amount of apatite (C).
Fig.11. IR spectra of dental calculi of human (A) consisting principally of CO_3-substituted apatite, CHA; of cat (B and C) a mixture of $CaCO_3$ and CHA; and dog (D) which contains a greater amount of $CaCO_3$ than the cat samples (B, C). The CO_3 vibration band for $CaCO_3$ is different from those of CO_3 in CHA [19,32].

Infrared absorption analyses

IR absorption spectra of human dental calculus (Fig. 11A) show the characteristic spectra of CHA (Fig. 3d) in which CO_3 has been partially substituted for PO_4^{3-}, coupled with the partial substitution of Na for Ca [19,24,32,33]. The IR spectra of specimens from cats (Figs. 11B,11C) show a greater amount of CHA than $CaCO_3$ compared to that of the dog (Fig. 11D). The dental calculi from tiger also showed a mixture of CHA and calcite.

Both x-ray diffraction and IR absorption analyses confirm the suggested results from the combined SEM and semi-quantitative microanalyses, namely, presence of several types of calcium phosphates in human dental calculi (Table 3, Figs. 9,10A) and presence of $CaCO_3$ mixed with CHA in animal (cat, dog, tiger) calculi (Table 3, Figs. 10B,C; 11B,C,D).

Discussion

This study demonstrates, for the first time, some morphological features of animal dental calculi. More importantly, it demonstrates the usefulness of combined SEM and semi-quantitative microanalyses in the identification of the crystalline constituents of human and animal dental calculi, and the confirmation of identification by both x-ray diffraction and IR absorption analyses.

Morphological features of human and animal dental calculi are similar in terms of the following: (a) presence of different shapes of calcified microorganisms: filaments, rods and cocci in human subgingival calculi, and predominantly rods in animal supra-gingival calculi (Figs. 5b, c, d, f, and 6a, b, c); (b) presence of channels or pores reflecting the forms (rods, cocci) of the microorganisms which "escaped" calcification (Figs. 5d, 6d); (c) two types of centers of mineralization: associated (Figs. 5b, c, f, 6b, c) and non-associated with bacteria (Figs. 5d, e, f, g, h, i, 6d, e, f, g) similar to the mineralization centers reported by Schroeder using TEM [46] and Lustman et al, using SEM [37]; (d) layered appearance indicating intermittent growth [20]; (e) presence of different shapes of crystalline components in human dental calculi: aggregates of short plate-like crystals or fan-like formation (Figs. 5e, f, h) similar to those shown earlier (but not identified) by Kerebel [17,18] and Jones [14]; cuboidal crystals of various sizes and states of aggregation (Figs. 5g, i), dense masses (Figs. 5b, d); while the predominance of only cuboidal crystals of different sizes in dense mineralized areas in animal calculi (Figs. 6e, f, g, h). The morphological features of human dental calculi are similar to those reported before [1,7,14,15-18,37-39,44-46].

The presence of cuboidal crystals in human dental calculi reported by Kerebel [17,18] was vaguely discounted as possible artifacts by Lustman et al [37]. This study shows that these cuboidal crystals, when, present in human dental calculi, are Mg-substituted tricalcium phosphates or whitlockites, β-TCMP, based on the morphological similarities with synthetic β-TCMP (Figs. 4h, 4i compared with Figs. 5g, 5i); and the presence of Mg correlates with Ca/P molar ratios 1.3 to 1.5 (Fig. 8). Similar cuboidal crystals found in arrested dentin caries [3,48,50] have been identified as β-TCMP using electron diffraction [3]. The correlation of Mg with Ca/P in human dental calculi, and the lack of correlation in animal dental calculi (Fig. 8) further supports the presence of β-TCMP in human but not in animal dental calculi. The suggestion of the presence of β-TCMP in human dental calculi and its absence in animal dental calculi based on microanalyses (Table

3) is confirmed by x-ray diffraction analyses (Figs. 9, 10).

Magnesium present in animal dental calculi may be associated with the apatite component since Mg is known to incorporate in apatite to a limited extent [21]. β-TCMP on the other hand, can incorporate as much as 2.7 wt % Mg [19,20,29,30,42,43]. Mg in human dental calculi is principally associated with the β-TCMP component [20]. Incorporation of Mg in an amorphous calcium phosphate phase in animal calculi is also a possibility. The absence of β-TCMP in animal dental calculi maybe due to the abundance of CO_3^{2-} in the oral environment which could suppress the formation of CHA [19,24,27] or even promote the formation of Mg-containing amorphous calcium phosphate [19,24]. Mg can also be associated with the calcite phase, forming a dolomite-type compound, $(Ca,Mg)(CO_3)_2$.

The difference in the distribution of the Ca/P molar ratios between human and animal dental calculi (Fig. 8) suggest the dominance of calcium phosphates (Ca/P, 1.3 to 1.8) in human and the dominance of non-phosphatic calcium compound in the animal calculi. Since previous studies of some animal dental calculi (dog, sheep, miniature pig), using x-ray diffraction and IR absorption analyses [26,51], showed the presence of calcite type $CaCO_3$, it is reasonable to assume that this non-phosphatic calcium compound, giving a very high Ca/P, is principally $CaCO_3$ (Table 3). This assumption is proven correct by x-ray diffraction (Figs. 10b, c, d) and IR absorption (Fig. 11) studies.

The differences in the crystalline components between human and animal calculi reflect the differences in the composition and pH of their oral environments [26]: the higher pH and higher carbonate / phosphate (C/P) molar ratios in dog (average pH 8.5, C/P about 180 for submaxillary) favors the formation of $CaCO_3$ and poorly crystalline apatite [19, 26]; while the lower pH and lower C/P in human saliva (average pH, 7; C/P about 3 in unstimulated saliva) favor the formation of different types of calcium phosphates (e.g., DCPD, OCP, CHA). An increase in the Mg levels in the human oral environment [4,47] above a critical Mg/Ca (e.g., above 0.1) will cause the formation of β-TCMP at the expense of CHA as shown in Fig. 2 [19,20,21,24,27,30,43]. Thus the crystalline components of human calculi (i.e., different types of calcium phosphates) and of animal calculi (i.e., $CaCO_3$ mixed with CHA but not other calcium phosphates) reflect the condition (pH) and composition of their oral environments. In vitro experiments have shown that when Ca-containing solution was added to human saliva, apatite was precipitated; while calcite was precipitated from the dog saliva [26]. The formation of the calcite form of $CaCO_3$ rather than other types of calcium carbonates (e.g., aragonite) was attributed to the presence of phosphate in dog saliva, since the presence of phosphate was shown in vitro to promote the formation of calcite, its absence, the formation of aragonite [26]. The co-existence of CHA with $CaCO_3$ in animal dental calculi may be due to the direct formation of CHA, or due to the partial transformation of $CaCO_3$ to CHA or both. Such transformations of $CaCO_3$ to CHA have been observed in vitro [28].

While x-ray diffraction and IR absorption analyses give more precise identification of the crystalline components in dental calculi compared to SEM / microanalyses, the former (x-ray diffraction and IR) provide global composition (mixture of crystal types) from macro areas. In contrast microanalyses cover micro areas comparable to some extent to the areas covered by microdiffraction [16], TEM [3,8,44,46] and electron diffraction [18, (RZ LeGeros, G Daculsi, in preparation)]. In addition, SEM has a definite advantage over TEM on the analyses of OCP since SEM can demonstrate the presence of OCP by comparing the morphology of the crystals in the specimen to those of synthetic OCP (Figs. 4d, e, f, g) combined with Ca/P molar ratio obtained by microanalyses (i.e. Ca/P close to 1.3). TEM cannot easily demonstrate the presence of OCP since the electron beam in TEM causes the transformation of OCP to apatite [44, (G Daculsi and RZ LeGeros, unpublished results)]. However, it should be noted that identification of crystals by SEM morphology alone is not sufficient and can even be misleading since crystal morphology is affected by different elements simultaneously present with the calcium and phosphate ions in the media from which the crystals form. For example, DCPD usually forms as triangular plates (Fig. 4a) from solutions or silica gel systems containing only calcium and phosphate ions; in the presence of pyrophosphate or when grown in agar gels, DCPD grow as aggregates of rods resembling OCP (Figs. 4b, c) [23-25,31]. It should also be noted that although microanalysis can give only semi-quantitative data at best when bulk rather than sectioned specimens are examined, careful interpretation of data [40], as was done in this study makes it a useful tool in combination with SEM in the identification of types of calcium compounds present in the dental calculi.

In conclusion, this study has demonstrated that by carefully considering the morphology and Ca/P molar ratios of synthetic calcium phosphates and existing knowledge about the crystalline components of human and some animal dental calculi, SEM combined with microanalyses can be very useful in the identification of the crystalline composition of human and animal dental calculi.

Acknowledgements

The professional collaboration of Dr. D. Lee (Harvard Medical School, Children's Hospital) for the SEM of synthetic $CaCO_3$ and β-TCMP and confirmatory SEM of some specimens; the valuable assistance of I. Jans (Nantes) in SEM/microanalyses; of H. Bleiwas in computer data analyses and graphics of microanalyses data; and of G. Marlino and M. Vaccaro (photography), are gratefully acknowledged. The authors are grateful to Dr. E.P. Dolensek (Director, Animal Health, NY Zoological Society), Dr. M. Marder (Manhattan Veterinary Group) and R. Moretti (NY Zoological Society) for the samples of calculi from cats, dogs and a tiger. This work was supported by National Institutes of Health (NIH/NIDR) research grant Nos. DE-04123 and DE-07223.

References

1. Bercy P, Frank RM (1980). Microscopie electronique a balayage de la plaque dentaire et du tartre a la surface du cement humain. J. Biol. Buccale. 8:299-313.

2. Canis MF, Kramer GM, Pamijer CM (1979). Calculus attachment, review of the literature and

new findings. J. Periodontol. 50:406-415.

3. Daculsi G, LeGeros RZ, Jean A, Kerebel B (1987). Possible physico-chemical processes in human dentin caries. J. Dent. Res. 66:1356-1359.

4. Dawes C, Jenkins GN (1964). The effects of different stimuli on the composition of saliva in man. J. Physiol. 170:86-100.

5. Forsberg A, Lagergreen C, Longerblad T (1960). Dental calculus--a biophysical study. Oral Surg. 13:1051-1060.

6. Fowler BO, Moreno EC, Brown WE (1966). Infrared spectra of hydroxyapatite, octacalcium phosphate and pyrolysed octacalcium phosphate. Arch. Oral Biol. 11:477-492.

7. Friskopp J, Hammarstrom L (1980). A comparative scanning electron microscopic study of supra-gingival and sub-gingival calculus. J. Periodontol. 51:553-562.

8. Gonzales F, Sognnaes RF (1960). Electron microscopy of dental calculus. Science 131:157-158.

9. Gron P, van Campen GJ, Lindstrom I (1967). Human dental calculus: inorganic, chemical and crystallographic composition. Arch. Oral Biol. 12:829-837.

10. Hoyer I, Gaengler P, Bimber R (1984). In vivo remineralization of human enamel and dental calculus formation. J. Dent. Res. 63:1136-1139.

11. Jenkins GN (1978). The Physiology and Biochemistry of the Mouth. 4th Ed., Blackwell Scientific Publications, Oxford. pp. 400-409.

12. Jenkins AT, Dano M (1954). Crystallography of dental calculus and the precipitation of certain calcium phosphates. J. Dent. Res. 33:741-750.

13. Jenkins AT, Rowles SL (1957). Magnesium whitlockite, a major constituent of dental calculus. Acta. Odont. Scand. 16:121-126.

14. Jones SJ (1972). Morphology of calculus formation on the human tooth surface. Proc. Roy. Soc. Med. 65:903-905.

15. Jones SJ (1987). The root surface: an illustrated review of some SEM studies. Scanning Microsc. 1:2003-2018.

16. Kani T, Kani M, Moriwaki Y, Doi Y (1983). Microbeam x-ray diffraction analysis of dental calculus. J. Dent. Res. 62:92-95.

17. Kerebel B (1971). Du microscope electronique a balayage a l'histologie et a la pathologie dentaires. Actualities Odonto-Stomatol. 96:449-472.

18. Kerebel B (1972). Ultrastructure due tartre au microscope electronique a balayage. Sci. et Recherche Odcnt. 2:27-33.

19. LeGeros RZ (1967). Crystallographic studies on the carbonate substitution in the apatite structure. PhD Thesis, New York University.

20. LeGeros RZ (1974). Variations in the crystalline components of human dental calculus: I. Crystallographic and spectroscopic methods of analysis. J. Dent. Res. 53:45-50.

21. LeGeros RZ (1984). Incorporation of magnesium in synthetic and biological apatites. In: Tooth Enamel IV, Fearnhead RW, Suga S (Eds.), Elsevier Science Publisher, Amsterdam. pp. 32-36.

22. LeGeros, RZ (1985). Preparation of octacalcium phosphate (OCP): A direct fast method. Calcif. Tissue Res. Int. 37:194-197.

23. LeGeros RZ, LeGeros JP (1972). Brushite crystals grown by diffusion. J. Crystal. Growth. 13:476-480.

24. LeGeros RZ, LeGeros JP (1984). Phosphate minerals in human tissues. In: Phosphate Minerals, Nriago J, Moore P (Eds). Springer-Verlag, Berlin. pp. 351-385.

25. LeGeros RZ, Morales P (1973). Renal stone crystals grown in gel systems. Invest. Urol. 11:12-20.

26. LeGeros RZ, Shannon IL (1979). The crystalline components of dental calculi: human vs. dog. J. Dent. Res. 58:2371-2377.

27. LeGeros RZ, Abergas T, Kijkowska R (1987). Formation of Mg-substituted whitlockite (β-TCMP). J. Dent. Res. 66:218. Abstract No. 896.

28. LeGeros RZ, Go P, Quirolgico GB, LeGeros DJ. (1980). Transformation of calcium carbonate and calcium phosphates to carbonate apatites: possible mechanisms for phosphorite formation. In: Proc. 2nd International Cong. on Phosphorus Compounds, Boston. pp. 40-57 (copy available from RZ LeGeros).

29. LeGeros RZ, Kijkowska R, LeGeros JP (1984). Formation and transformation of octacalcium phosphate, OCP: a preliminary report. Scanning Electron Microsc. 1984;II:1771-1777.

30. LeGeros RZ, Klein E, Miravite MA (1974). Biological whitlockites, occurrence and formation. J. Dent. Res. 53:199 (abstract).

31. LeGeros RZ, Lee D, Quirolgico G, Shrira WP, Reich L (1983). In vitro formation of dicalcium phosphate dihydrate. Scanning Electron Microsc. 1983;I:407-418.

32. LeGeros RZ, LeGeros JP, Trautz OR, Klein E (1970). Spectral properties of carbonate in carbonate-containing apatites. Dev. App. Spec. 78:3-12.

33. LeGeros RZ, LeGeros JP, Trautz OR, Shirra WP (1971). Conversion of monetite, $CaHPO_4$ to apatites: effect of carbonate on the crystallinity and the morphology of apatite crystallites. Adv. X-ray Anal. 14:57-66.

34. LeGeros RZ, Singer L, Ophaug R, LeGeros JP (1982). The effect of fluoride on the stability of synthetic and biological (bone mineral) apatites. In: Osteoporosis, Menczel J, Robin GC, Makin M (Eds). J. Wiley & Sons, New York. pp. 327-341.

35. LeGeros RZ, Taheri MH, Quirolgico GB, LeGeros JP (1980). Formation and stability of apatites: effects of some cationic substituents. In: Proc. 2nd International Cong. on Phosphorus Compounds, Boston. pp. 89-103 (copy available from RZ LeGeros).

36. Little MF, Casciani CA, Rowley J (1963). Dental calculus composition. I: Supra-gingival calculus: ash, calcium, phosphorus, sodium, and density. J. Dent. Res. 42:78-82.

37. Lustman J, Lewin-Epstein J, Shteyer A (1976). Scanning electron microscopy of dental calculus. Calcif. Tissue Res. 21:47-55.

38. Mandel ID, Levy BM (1957). Studies on salivary calculus. I. Histochemical and chemical investigations of supra- and sub-gingival calculus. O.S., O.M. & O.P. 10:874-884.

39. Moskow BS (1969). Calculus attachment in cemental separation. J. Periodontol. 40:125-130.

40. Nelson AC, Schoen FG, Levy RG (1985). Scanning electron microscopy methodology for the study of pathophysiology of calcification of bioprosthetic heart valves. Scanning Electron Microsc. 1985;I:209-213.

41. Newesely H (1968). Calcifying processes within superficial layers of dental plaque. Caries Res. 2:19-24.

42. Rowles SL (1964). The inorganic composition of dental calculus. In: Bone and Tooth, Blackwood HJJ (Ed.), Pergamon Press, London. pp. 175-183.

43. Rowles SL (1967). The precipitation of whitlockite from aqueous solutions. Coll. Int. sue les Phosphates Mineraux Solides., Society Chimique de France, 1:151-155.

44. Saxton CA (1968). Identification of octacalcium phosphate in human dental calculus by electron diffraction. Arch. Oral. Biol. 13:243-246.

45. Saxton CA (1973). Scanning electron microscope study of the formation of dental plaque. Caries Res. 7:102-119.

46. Schroeder H (1969). Formation and Inhibition of Dental Calculus. Hans Huber, Berne. pp. 100-122.

47. Shannon IL (1974). Saliva: composition and secretion. In: Monographs in Oral Science, Vol. 2, S. Karger, Basel. pp. 3-42.

48. Takuma S, Ogiwara H, Suzuki H (1975). Electron probe and electron microscope studies of carious dentinal lesions with remineralized surface layer. Caries Res. 9:278-285.

49. Trautz OR, Fessenden E (1958). Formation and stability of whitlockite and octacalcium phosphate, two components of salivary calculi. J. Dent. Res. 37:78 (abstract).

50. Vahl J, Hohling HJ, Frank R (1964). Elektronenstrahlenbeugung und rhombohedrisch aussehendedn mineralbildugen kariosem dentin. Arch. Oral Biol. 9:315-320.

51. Weaver ME (1964). X-ray diffraction study of calculus of miniature pig. Arch. Oral Biol. 9:75-81.

52. Zander HA (1953). The attachment of calculus to root surfaces. J. Periodont. 24:16-19.

Discussion with Reviewers

P.T. Cheng: What is the conclusive evidence that the cuboidal crystals observed in dental calculi are actually whitlockite crystals?
Authors: Morphology (SEM), Mg/Ca, Ca/P (microanalyses) suggested the presence of whitlockite. X-ray diffraction pattern showing β-TCMP (characterized by shorter a-axis due to Mg-for-Ca substitution in the whitlockite structure) confirmed its presence.

P.T. Cheng: Why is the morphology of the synthetic whitlockite crystals so different from that observed in dental calculi?
Authors: Whitlockite or β-TCMP crystals were found only in human and not in animal dental calculi. Their sizes and state of aggregations vary (Figs. 5g, 5i). Their morphology is similar to those of synthetic β-TCMP (Figs. 4h, 4i).

Reviewer III: What is known about the saturation levels of the salivas with respect to calcium phosphates and calcium carbonate?
Authors: Unstimulated human saliva is supersaturated with respect to DCPD, OCP and apatite [Gron P (1973): Arch. Oral Biol. 18: 1385-1392]. In vitro studies showed that human saliva (unstimulated) is supersaturated with respect to CHA; dog saliva, with respect to $CaCO_3$ (calcite form) [26].